

An analytical model for the non-linear redshift-space power spectrum

Xi Kang¹, Y.P. Jing^{1,2}, H. J. Mo², and G. Börner²

¹Shanghai Astronomical Observatory, the Partner Group of MPI für Astrophysik, Nandan Road 80, Shanghai 200030, China

²Max-Planck Institut für Astrophysik, Karl-Schwarzschild-Strasse 1, 85748 Garching, Germany

Email: kangx@center.shao.ac.cn, yypjing@center.shao.ac.cn, hom@mpa-garching.mpg.de, grb@mpa-garching.mpg.de

1 February 2008

ABSTRACT

We use N-body simulations to test the predictions of the redshift distortion in the power spectrum given by the halo model in which the clustering of dark matter particles is considered as a result both of the clustering of dark halos in space and of the distribution of dark matter particles in individual dark halo. The predicted redshift distortion depends sensitively on several model parameters in a way different from the real-space power spectrum. An accurate model of the redshift distortion can be constructed if the following properties of the halo population are modelled accurately: the mass function of dark halos, the velocity dispersion among dark halos, and the non-linear nature of halo bias on small scales. The model can be readily applied to interpreting the clustering properties and velocity dispersion of different populations of galaxies once a cluster-weighted bias (or equivalently an halo occupation number model) is specified for the galaxies. Some non-trivial bias features observed from redshift surveys of optical galaxies and of IRAS galaxies relative to the standard low-density cold dark matter model can be easily explained in the cluster weighted bias model. The halo model further indicates that a linear bias can be a good approximation only on for $k \leq 0.1 h \text{Mpc}^{-1}$.

Key words: Galaxy clustering - galaxies: distances and redshifts - large-scale structure of Universe - cosmology: theory - dark matter

1 INTRODUCTION

The power spectrum of the galaxy spatial distribution is an important statistic for describing inhomogeneities in the Universe. The spatial distribution of galaxies observed with a redshift survey is distorted by the peculiar motions of galaxies, and a statistically isotropic distribution (e.g. the power spectrum or the correlation function) in real space becomes anisotropic in redshift space (Geller & Peebles 1973; Davis & Peebles 1983; Bean et al. 1983; Kaiser 1987). On the other hand, when measuring clustering for high redshift objects in redshift space, choosing the wrong cosmological model can lead to an additional anisotropy in the redshift space distribution (Matsubara & Suto 1996; Ballinger, Peacock & Heavens 1996). The theory for the redshift distortions caused by an assumed world model and by the large scale linear motions is now well established. The transform of the clustering pattern from the true world model to an assumed model is just a simple mapping in the coordinates. On large scales and for a linear bias, the redshift power spectrum $P_l^S(k, \mu)$ can be derived (Kaiser 1987)

$$P_l^S(k, \mu) = P_l^R(k) [1 + \beta \mu^2]^2 \quad (1)$$

where μ is the cosine of the angle between the line-of-sight and the \mathbf{k} vector, $\beta = \Omega^{0.6}/b$, Ω the density parameter, b the linear bias, and $P_l^R(k)$ the linear power spectrum of dark matter in real space. The hope has been to measure the dynamical quantity β and the cosmological parameters through studying the anisotropy of galaxies or galaxy cluster on large enough scales. However, it has been shown that the virialized motions within rich clusters (the Finger-of-God effect) are so prominent that the clustering pattern on large scales of wave number $k \sim 0.1 h \text{Mpc}^{-1}$, is significantly affected (Cole, Fisher & Weinberg 1994; Suto et al. 1999). The effect of non-linear motions on the redshift distortion must be properly modelled in order to measure the dynamical quantity and the cosmological parameters from the redshift distortion of extragalactic objects. Recent results (Peacock et al. 2001) from the redshift distortion of the 2dF galaxies further support this point, as even with the largest redshift survey available today there exists a tight degeneracy in the determinations of the parameters β and the pairwise velocity σ_v (reflecting the non-linear motion). As pointed out recently by Jing & Börner (2001, hereafter JB2001), the existing analytical model for the nonlinear ve-

locity distortion, e.g. the exponential distribution of the relative velocity in coordinate space (Davis & Peebles 1983) or the Lorentz damping function in k-space (Cole, Fisher & Weinberg 1995; Peacock & Dodds 1994), is at best an approximation for some scales. Although JB2001 have made an extensive study of the redshift distortion for the dark matter and for two specific biased tracers in three typical cosmological models based on high-resolution simulations, it is unknown how to generalize their results to cosmological models and/or to biased tracers different from those studied in their work without running new simulations. In this paper, we present an analytical model for the redshift distortion based on the halo model, and we will test the accuracy of the analytic model with the results of JB2001.

A key concept in the standard hierarchical scenario of structure formation is the formation of dark matter halos, which are virialized systems of dark matter particles formed through non-linear gravitational collapse in the cosmic density field. Since the formation of dark halos involves only gravitational physics, accurate analytic models are now available for many properties of the halo population, such as the mass function (Press & Schechter 1974; Lee & Shandarin 1998; Sheth & Tormen 1999; Sheth, Mo & Tormen 2001), clustering properties, (Mo & White 1996; Mo, Jing & White 1997; Jing 1998, 1999; Sheth & Tormen 1999; Sheth, Mo & Tormen 2001; Hamana et al. 2001), and density profiles (Navarro, Frenk & White 1996, 1997; Moore et al. 1999; Jing & Suto 2000; Klypin et al. 2001). Such models are very useful in understanding the clustering properties of matter in the universe, as well as in understanding the bias of the galaxy distribution relative to the underlying density field. Indeed, since in the hierarchical cosmogony all masses in the universe are partitioned in dark halos, the halo clustering properties, the halo mass function and the halo density profiles are sufficient for the construction of a clustering model for the dark matter in the universe (Scherrer & Bertschinger 1991; Sheth & Jain 1997; Ma & Fry, 2000a,b; Seljak 2000; Cooray, Hu & Miralda-Escude 2000; Cooray 2001). Furthermore, since galaxies are assumed to form through gas cooling and condensation in dark halos, a halo model of galaxy clustering can also be constructed by combining the clustering properties of the halo population with an assumption of how galaxies populate dark halos (Jing, Mo & Börner 1998; Peacock & Smith 2000; Seljak 2000; Scoccimarro & Sheth 2001; Scoccimarro et al. 2001; Berlind & Weinberg 2001).

The halo model also provides a useful way to understand the redshift distortion in galaxy clustering (Seljak 2001; White 2001). In this model, the enhancement of the redshift-space power spectrum (relative to that in real space) on large scales is assumed to arise in the halo-halo correlation, while the smearing (Finger-of-God) effect on small scales is attributed to the velocity dispersions in dark halos. In this paper we show, however, that the redshift distortion depends on several important effects which were not included in early modelling. Using results derived from high-resolution N-body simulations we show that an accurate model for the redshift distortion depends not only on the mass function of dark halos, the dark halo clustering and the velocity dispersion among dark halos, but also on the nonlinear motion of halos at intermediate scales.

2 POWER SPECTRUM IN REAL SPACE

In the halo model, the mass density field in the Universe is a superposition of halos distributed in space. The mass function $\phi(M) dM$ of halos (which is the mean density of halos with mass in the range of $[M, M + dM]$) and their spatial distributions $n(M, \mathbf{r}) dM$ (which is the number density of halos with mass in the range of $[M, M + dM]$ at position \mathbf{r}) can be described by the extended Press-Schechter formalism (Press & Schechter 1974; Bond et al. 1991; Bower 1991; Mo & White 1996) or its empirical fitting formula from N-body simulations (Jing 1998, 1999; Sheth & Tormen 1999). Assuming the density profile of halos to be $\rho_\alpha(M, \mathbf{r})$ for mass M , the density in the Universe can be expressed as

$$\rho(\mathbf{r}) = \int n(M, \mathbf{r}_1) \rho_\alpha(M, |\mathbf{r} - \mathbf{r}_1|) dM d^3 \mathbf{r}_1. \quad (2)$$

Following Peebles (1980) and Scherrer & Bertschinger (1991), we can divide the 4-dimensional space of \mathbf{r} and M into infinitesimal volume elements so that the occupation number n_i of halos within any of the volume elements is either 0 or 1. Then the density field can be written as,

$$\rho(\mathbf{r}) = \sum_i n_i \rho_\alpha(M_i, |\mathbf{r} - \mathbf{r}_i|). \quad (3)$$

Using the following relations

$$\begin{aligned} \langle n_i \rangle &= \langle n_i^2 \rangle = \phi(M_i) dM_i d^3 \mathbf{r}_i, \\ \langle n_i n_j \rangle_{i \neq j} &= \phi(M_i) \phi(M_j) [1 + \xi(r_{ij})] d^3 \mathbf{r}_i d^3 \mathbf{r}_j dM_i dM_j, \end{aligned} \quad (4)$$

where $r_{ij} = |\mathbf{r}_i - \mathbf{r}_j|$, we can derive the two-point correlation function $\xi(r)$ for the density field which is a sum of two terms,

$$\xi(r) = \xi_{1h}(r) + \xi_{2h}(r) \quad (5)$$

where the first term on the *rhs* is the so-called one-halo term $\xi_{1h}(r)$ which is contributed by the internal halo structure (the density profile) and the second term is the two-halo term $\xi_{2h}(r)$ which is contributed by the halo-halo clustering (Ma & Fry 2000b):

$$\begin{aligned} \bar{\rho}^2 \xi_{1h}(r) &= \int d^3 \mathbf{r}' \int dM \phi(M) \rho_\alpha(M, r') \rho_\alpha(M, |\mathbf{r}' + \mathbf{r}|), \\ \bar{\rho}^2 \xi_{2h}(r) &= \int d^3 \mathbf{r}' d^3 \mathbf{r}'' \left[\int dM_1 \phi(M_1) \rho_\alpha(M_1, r') \right] \\ &\quad \times \left[\int dM_2 \phi(M_2) \rho_\alpha(M_2, r'') \right] \\ &\quad \times \xi_{hh}(|\mathbf{r}' - \mathbf{r}'' + \mathbf{r}|, M_1, M_2). \end{aligned} \quad (6)$$

In the above equation, $\bar{\rho}$ is the mean mass density and $\xi_{hh}(r, M_1, M_2)$ is the two-point correlation function of halos of mass M_1 and mass M_2 . In k-space, using $\tilde{\rho}_\alpha(M, k)$ to denote the Fourier transform of $\rho_\alpha(M, r)$, where $\tilde{\rho}_\alpha(M, k) = \int_0^\infty d^3 \mathbf{r} \rho_\alpha(M, r) e^{-i\mathbf{k} \cdot \mathbf{r}}$, we can derive the mass power spectrum $P(k)$,

$$\begin{aligned} P(k) &= P_{1h}(k) + P_{2h}(k), \\ \bar{\rho}^2 P_{1h}(k) &= \int dM \phi(M) \tilde{\rho}_\alpha^2(M, k), \\ \bar{\rho}^2 P_{2h}(k) &= \int dM_1 \phi(M_1) \tilde{\rho}_\alpha(M_1, k) \int dM_2 \phi(M_2) \tilde{\rho}_\alpha(M_2, k) \\ &\quad \times P_{hh}(k, M_1, M_2) \end{aligned} \quad (7)$$

Where $P_{hh}(k, M_1, M_2)$ is the Fourier transform of $\xi_{hh}(r, M_1, M_2)$, that is the cross power spectrum of the halos of mass M_1 and M_2 . In the halo model, the mass power spectrum or the mass correlation function is fully determined by the halo mass function $\phi(M)$, the halo mass density profile $\rho_\alpha(M, r)$ and the halo-halo power spectrum.

The halo mass function $\phi(M)$ is given by the Press-Schechter formula,

$$\phi(M) = \left[\frac{2}{\pi} \right]^{1/2} \left| \frac{d \ln \sigma(M)}{d \ln M} \right| \frac{\bar{\rho}}{M} \nu e^{-\nu^2/2}, \quad \nu = \frac{\delta_c}{\sigma(M)} \quad (8)$$

where δ_c is a parameter characterizing the linear overdensity at the onset of gravitational collapse, which is 1.686 in the case of a spherical collapse model in an Einstein-de Sitter universe and depends weakly on cosmological models. The rms linear mass fluctuation $\sigma(M)$ in spheres of radius R is related to the linear power spectrum $P_{lin}(k)$

$$\sigma^2(M) = \int_0^\infty \frac{4\pi k^2 dk}{(2\pi)^3} P_{lin}(k) W^2(kR) \quad (9)$$

where $W(x) = 3(\sin x - x \cos x)/x^3$ is the Fourier transform of a real-space top-hat window function.

We take the following form

$$\frac{\rho_\alpha(r)}{\bar{\rho}} = \frac{\bar{\delta}}{(r/R_s)^p (1 + r/R_s)^{3-p}} \quad (10)$$

for the density profile of halos in CDM cosmological models. In the above equation, $\bar{\delta}$ is a dimensionless density amplitude, and R_s is a scale radius. The seminal work of Navarro, Frenk, & White (1996, 1997; NFW) showed that the halos formed in CDM models can all be well described by equation (10) with $p = 1$. Subsequent work with higher numerical resolution has shown that the innermost density profiles of the halos are steeper than the NFW form especially for the halos of galactic mass (Fukushige & Makino 1997; Moore et al. 1998; Jing & Suto 2000; Fukushige & Makino 2001), and the profiles are better described by $p = 1.5$. Defining the radius of a halo, R_{200} , such that within it the mean matter density is 200 times the mean density, the density profile is characterized by the two parameters p and the concentration parameter $c = R_{200}/R_s$. The concentration parameter was found to depend on the halo mass, and can be computed for $p = 1$ semi-analytically (NFW). In this paper, we will use the following fitting formula

$$\begin{aligned} c(M) &= 7.0 \left(\frac{M_*}{M} \right)^{\frac{1}{6}}, & p = 1, \\ c(M) &= 3.5 \left(\frac{M_*}{M} \right)^{\frac{1}{6}}, & p = 1.5, \end{aligned} \quad (11)$$

for the LCDM model which fits well the concentration parameters measured by Jing & Suto (2000) for this model (see also Lokas 2001). A simple fit to the concentration parameters of SCDM halos in NFW gives

$$c(M) = 10 \left(\frac{M_*}{M} \right)^{0.09}, \quad p = 1.0. \quad (12)$$

and as for the LCDM, the concentration for $p = 1.5$ is 0.5 times of that for $p = 1$. The mass of a halo M is related to R_{200} simply by $M = \frac{800\pi}{3} R_{200}^3 \bar{\rho}$, and M_* is defined by requiring $\sigma(M_*) = \delta_c$.

The halo distribution is assumed to be linearly biased relative to the underlying mass distribution, that is the

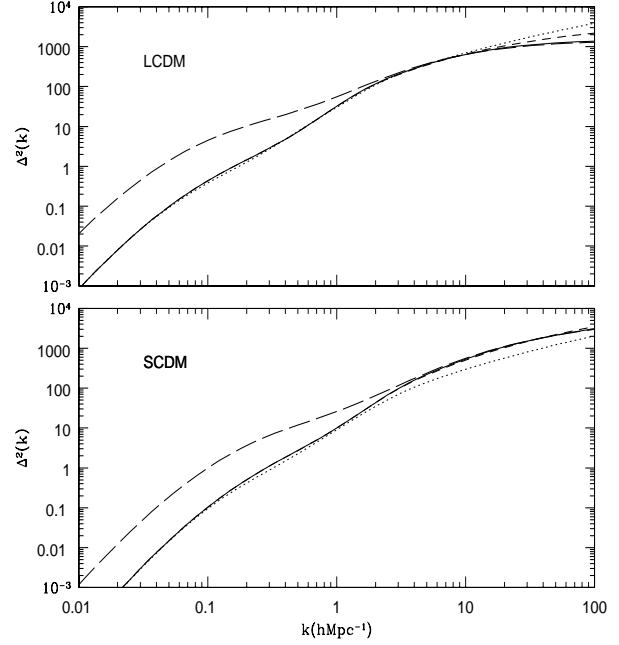


Figure 1. The real-space power spectrum of dark matter in the LCDM and SCDM models. The dotted line is the prediction based on the formula of Peacock & Dodds (1996), the solid (for $p = 1.0$) and the short-dashed (for $p = 1.5$) lines are the predictions of the halo model with the density profile cut at the radius R_{200} . The long-dashed line is the prediction of the halo model for the density profile of $p=1.0$ without a cutoff in radius

power spectrum $P_{hh}^R(k, M_1, M_2)$ is related to the mass power spectrum $P_{mass}(k)$

$$P_{hh}^R(k, M_1, M_2) = b(M_1)b(M_2)P_{mass}(k) \quad (13)$$

where $b(M)$ is the bias factor of halos for mass M . We will use the analytical formula derived by Mo & White (1996)

$$b(M) = 1 + (\nu^2 - 1)/\delta_c, \quad \nu = \delta_c/\sigma(M), \quad (14)$$

for the bias factor. Following Ma & Fry (2000b), we will use the linear density power spectrum $P_{lin}(k)$ for $P_{mass}(k)$, partly for simplicity but more importantly because it can partly account for the exclusion effect between halos. In §4, we test the accuracy of this assumption.

Now, consider two cosmological models. The LCDM model is a spatially flat model with matter density $\Omega_m = 0.3$ and cosmological constant $\Omega_\Lambda = 0.7$. Its linear power spectrum has the shape parameter $\Gamma = \Omega_m h = 0.2$ and the amplitude $\sigma_8 = 1$ (which is the rms mass density fluctuation in a top-hat window with radius $8h^{-1}$ Mpc). The SCDM model is a spatially flat model but without a cosmological constant. Its linear power spectrum has $\Gamma = 0.5$ and $\sigma_8 = 0.6$.

Figure 1 shows a comparison between the real-space power spectrum derived from the halo model and the fitting formula of Peacock & Dodds (1996; PD96) for the two cosmological models at redshift $z = 0$. First, we used the fitting formula of Ma & Fry (2000b) for the Fourier transform of the density profile $\tilde{\rho}_\alpha(M, k)$. When obtaining the fitting formula they apparently assumed that the density profile (equation 10) extends to infinity. With their fitting formula, we obtained the mass power spectrum for the LCDM model (the long-dashed line in the upper panel) which

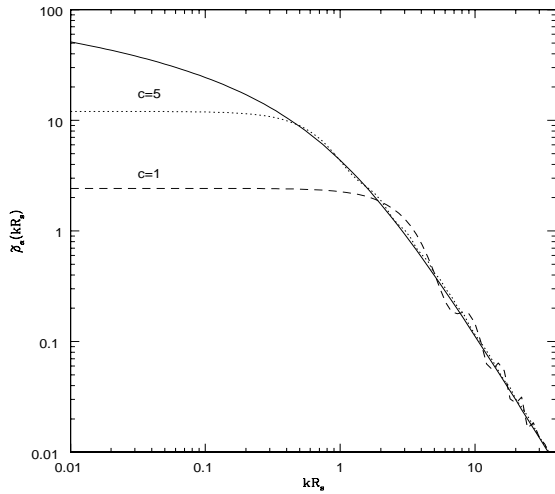


Figure 2. The Fourier transform of the density profile $\rho_\alpha(c, r)$. The dashed and the dotted lines are for $c=1$ and $c=5$ respectively with the density profile cutoff at radius R_{200} . For comparison, the solid line is the fitting formula of Ma & Fry (2001b) in which the density profile extends to the infinity

is in good agreement with the fitting formula of PD96 on small scales ($k \geq 2h^{-1}\text{Mpc}$), but has much more power on large scales. The reason is that the halo density profiles of equation (10) are assumed to extend to infinity, while there should be a radial cutoff in the halo structure (Sheth, Hui, Diaferio & Scoocimarro 2001). When we take R_{200} as the radial cutoff for the Fourier transform $\tilde{\rho}_\alpha(M, k) = \int_0^{R_{200}} d^3\mathbf{r} \rho_\alpha(M, r) e^{-i\mathbf{k}\cdot\mathbf{r}}$, we get a mass power spectrum which is in very good agreement with the fitting formula of PD96 both on small and on large scales in the LCDM model. The significance of the cutoff is illustrated in Figure 2 for $p = 1$, where we plot our computed $\tilde{\rho}_\alpha(M, k)$ against the algebraic expression without a cutoff of Ma & Fry (2000b) (the solid line). The radial cutoff brings about a flat $\tilde{\rho}_\alpha(M, k)$ at small k (large scale), significantly smaller than without a radial cutoff for $k < 1/R_{200}$. As we have seen from Figure 1, the radial cutoff is important to get the correct real-space power spectrum, and we will adopt this cutoff throughout the paper (A cutoff was also imposed in the work of Ma & Fry 2001a,b; C.P. Ma, private communications). For the SCDM model, the halo model prediction is 50 percent higher than the fitting formula of PD96 on small scales (for $k \geq 1h^{-1}\text{Mpc}$). A similar discrepancy is found for the LCDM model (the figure not plotted in the paper) if we replace $\bar{\rho}$ (equation 10) with ρ_{crit} and take R_{200} as the radius of a sphere of mean interior density $200\rho_{crit}$, where ρ_{crit} is the critical density of the universe. Therefore, the inaccuracy of the halo model prediction for the mass power spectrum is perhaps 50 to 100 percent (in contrast to many recent studies which claimed that the halo model is much more accurate). In a subsequent paper we will examine this issue in a greater detail by comparing the halo model with the results from high-resolution N-body simulations of 512^3 particles.

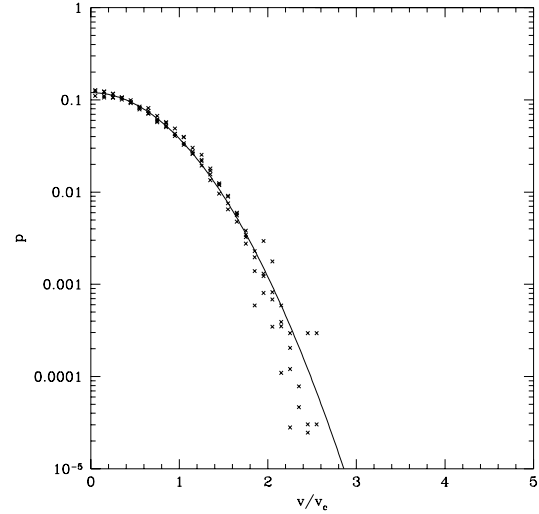


Figure 3. The 1-D velocity distribution of particles within virialized halos in simulations (symbols) is well described by a Maxwellian distribution with $\sigma_v^{1D}/V_{200} = 1/1.53$ (the solid line)

The mass power spectrum calculated in the halo model is quite insensitive to the choice of p for the innermost density profile. The difference in $P(k)$ between $p = 1$ and $p = 1.5$ is rather small for $k \leq 10h\text{Mpc}^{-1}$, and we will consider only $p = 1.5$ for the calculation of the redshift-space power spectrum below. We also found that the real-space power spectrum in the halo model is quite robust against a reasonable change of the mass function $\phi(M)$ and the linear bias factor $b(M)$. In contrast we will see that the red-shift power spectrum is quite sensitive to the changes of these functions.

3 THE POWER SPECTRUM IN REDSHIFT SPACE

The dark matter halo is nearly virialized inside R_{200} . The velocity distribution of the dark matter within the halo should be approximately Maxwellian distributed with a one-dimensional velocity dispersion σ_v^{1D} (Sheth 1996). We have tested this assumption with the N-body simulations of Jing & Suto (1998), and confirmed that the assumption is valid (see Figure 3). Furthermore, we found that

$$\sigma_v^{1D}/V_{200} \approx 1/1.53 \quad (15)$$

slightly smaller than $1/\sqrt{2}$, where $V_{200} = \sqrt{GM/R_{200}}$ is the circular velocity at the viral radius R_{200} , and M is the mass of the halo within R_{200} . The virial motion in the halo elongates the density distribution of the halo along the line-of-sight in redshift space. The density distribution of a halo in redshift space $\rho_\alpha^S(r_\pi, r_\sigma)$ is a convolution of the real-space density profile with the velocity distribution along the line-of-sight,

$$\rho_\alpha^S(r_\pi, r_\sigma) = \int \rho_\alpha(r_\pi - v_z/H, r_\sigma) f(v_z) dv_z, \quad (16)$$

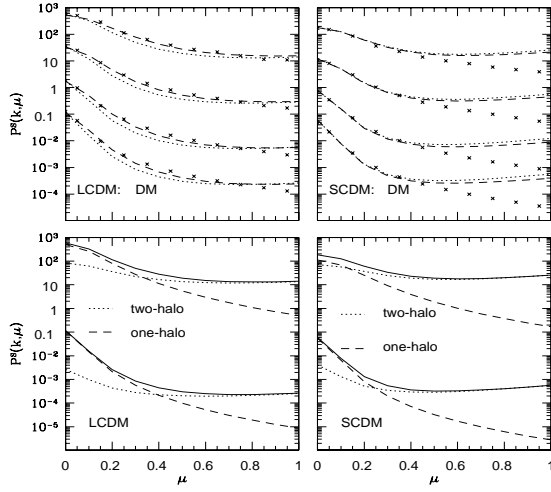


Figure 4. The redshift power spectrum of dark matter (dot lines in the upper panels) and contributions from the one-halo and the two-halo terms (the lower panels). The dashed lines in the upper two panels are the results after accounting for the finite size of the simulation box. The crosses are the simulation results of JB2001. In the upper panel, from top to bottom, the values of k are 1.1, 1.7, 2.7, and 3.4 hMpc^{-1} respectively, and the values $P^S(k, \mu)$ are multiplied by 1, 10^{-1} , 10^{-2} , and 10^{-3} respectively for clarity. For the halo model, the Press-Schechter formula, the formula of Mo & White (1996), and Kaiser's formula are used for the mass function of halos, the halo bias and the redshift distortion of halos. In the lower panel, the one-halo and two-halo contributions are drawn by dotted and dashed lines. Their sums are the solid lines. The wavenumber is 1.1 and 3.4 hMpc^{-1} for the upper and lower lines and the $P^S(k, \mu)$ values have been multiplied by 1 and 10^{-3} respectively for clarity.

where r_π and r_σ are the distances parallel and perpendicular to the line-of-sight to the halo center, H is the Hubble constant, and $f(v_z)$ is the velocity distribution along the line-of-sight. The redshift space power spectrum $P^S(k, u)$ can then be written as,

$$\begin{aligned} P^S(k, \mu) &= P_{1h}(k, \mu) + P_{2h}(k, \mu) \\ P_{1h}^S(k, \mu) &= \int dM \phi(M) \tilde{\rho}_\alpha^2(M, k) e^{-k^2 \mu^2 \sigma_v^{1D^2(M)}}, \\ P_{2h}^S(k, \mu) &= \int dM_1 \phi(M_1) \tilde{\rho}_\alpha(M_1, k) e^{-k^2 \mu^2 \sigma_v^{1D^2(M_1)/2}} \\ &\quad \times \int dM_2 \phi(M_2) \tilde{\rho}_\alpha(M_2, k) e^{-k^2 \mu^2 \sigma_v^{1D^2(M_2)/2}} \\ &\quad \times P_{hh}^S(k, \mu, M_1, M_2). \end{aligned} \quad (17)$$

Where $P_{hh}^S(k, \mu, M_1, M_2)$ is the redshift power spectrum for two dark matter halos with mass M_1 and M_2 . Under the assumption that every halo is moving as a whole according to linear theory (Kaiser 1987), we can derive the redshift power spectrum for halos,

$$\begin{aligned} P_{hh}^S(k, \mu, M_1, M_2) &= [1 + \Omega^{0.6} \mu^2 / b(M_1)] P_{hh}^R(k, M_1, M_2) \\ &\quad \times [1 + \Omega^{0.6} \mu^2 / b(M_2)]. \end{aligned} \quad (18)$$

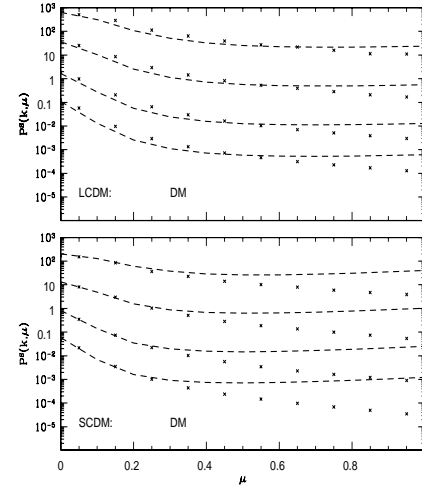


Figure 5. The same as the upper panels of Figure 4 but with the modified formulae for the halo mass function and the linear bias factor

We will show that the formula is a good description on large scales, but on small scales it gives too much power at large μ . A modified formula will be given in the next section.

In Figure 4 we plot the redshift power spectrum for dark matter based on this halo model, and compare it to the simulation results of JB2001 for the two cosmological models. From the dot line in the top panels, we see that the difference in the redshift power spectrum between the halo model and the simulations is small on large scales (i.e small k). But on small scales the halo model gives significantly more power at larger μ than the simulation data, especially in the SCDM model. It is also noted that the finite box size effect should be taken into account. In Figure 4 we also plot $P^S(k, \mu)$ (the dashed lines in the upper two panels) calculated using a cut-off of the power spectrum for a scale smaller than the box-size ($100h^{-1} \text{ Mpc}$ in our simulation). The value of $P^S(k, \mu)$ at larger μ are lower in the case, but the changes are quite small. The difference is so significant that we have to check all the assumptions used in our model: the halo mass function; the density profile of halos; and the halo-halo redshift power spectrum. Before doing that, it would be helpful first to check which term, the one-halo term or two halo term, is the main contribution to the discrepancy. From the lower panels of Figure 4, it can be easily found that the two-halo term dominates the redshift power spectrum at large μ even for small scales (k about a few hMpc^{-1}), in contrast to the real-space power spectrum (Ma & Fry 2000b). The reason for the difference is that the strong real-space clustering power from the one-halo contribution is suppressed by its internal motion, while the infall (merging) of halos to each other enhances the $P^S(k, \mu)$. We also find that the small halos contribute significantly to the two-halo term. As for the real-space power spectrum, we find that the density profile of dark matter has little effect on $P^S(k, \mu)$ for $k \leq 4 \text{ hMpc}^{-1}$ (the upper limits of k in our paper) for $1 \leq p \leq 1.5$. In the following section, we will check

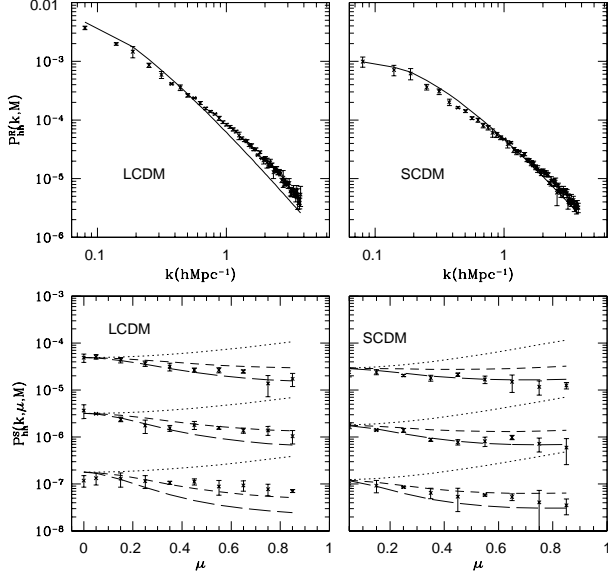


Figure 6. Upper panels – The real-space power spectrum of halos with mass $M = 1.75 \times 10^{11} h^{-1} M_{\odot}$ for the LCDM and $M = 6.0 \times 10^{11} h^{-1} M_{\odot}$ for the SCDM model measured from the N-body simulations (the symbols) compared with the formula of Eq.(13) (the solid lines). Lower panels – the redshift space power spectrum of halos in the simulations. The values of k are 1.4, 1.7 and 2.1 hMpc^{-1} respectively. The dotted, the dashed and the long-dashed lines are the predictions of equation (20) with $\sigma = 0, 200$, and 300 km s^{-1} and the nonlinear real-space power spectrum of halos. The $P_{hh}^S(k, \mu, M)$ values have been multiplied by 1, 10^{-1} , 10^{-2} respectively for clarity

the validity of the assumptions about the mass function and the halo-halo correlation.

4 MODIFICATIONS OF THE ASSUMPTIONS ABOUT THE HALO DISTRIBUTIONS

It has been shown by Jing (1998) and Lee & Shandarin (1998) that the Press-Schechter formula, equation (8) and equation (14) for the halo bias are not good descriptions for small halos in high resolution simulations. Actually the simulations produce fewer halos than the P-S formula in an intermediate mass range $0.2 \leq M/M_* \leq 1$, but more halos both for smaller and larger masses. Motivated by these findings, (Sheth & Tormen (1999)) have found the fitting formula for the mass function and the halo bias parameter (see also Sheth, Mo & Tormen 2001),

$$\begin{aligned} \phi(M) &= \frac{\bar{\rho}}{M^2} \frac{d \log \nu'}{d \log M} A \left[1 + \frac{1}{a \nu'^n} \left(\frac{a \nu'}{2} \right)^{1/2} \frac{e^{-a \nu'/2}}{\sqrt{\pi}} \right], \\ b(M) &= 1 + \frac{a \nu' - 1}{\delta_c} + \frac{2n/\delta_c}{1 + (a \nu')^n}, \end{aligned} \quad (19)$$

where $a = 0.707$, $n = 0.3$, $A = 0.32$ and $\nu' = (\delta_c/\sigma(M))^2$. We now take these formula and recalculate the redshift-space power spectrum for dark matter. The results are shown in Figure 5, where we can find that at small μ the agreement between the model and the simulation is im-

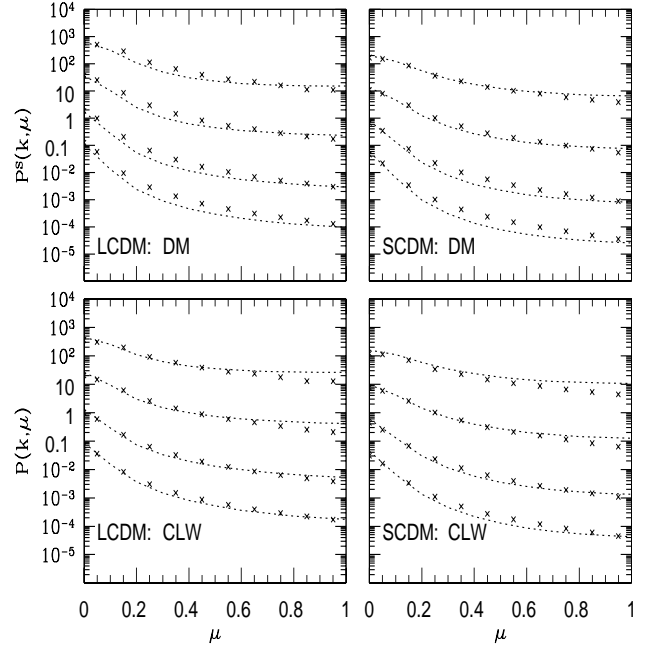


Figure 7. Upper panels – the same as Figure 5, but with the nonlinear motions of halos included in the halo model. The parameter σ is 200 km s^{-1} for the LCDM and 300 km s^{-1} for the SCDM model. Lower panels – the same as the upper panels but for galaxies described by the cluster weighted model

proved very moderately, but not at larger μ . The results can be explained as follows: the modified formulae for the halo mass function and the halo bias give a higher number density and a higher bias factor for small halos (which have mass less than $10^{11} M_{\odot}$) than the P-S and Mo & White formulae used in the last section, both of which boost the two-halo term of the real-space power spectrum. While the linear redshift compression due to the Kaiser effect (which increases the redshift power spectrum) is reduced by a larger bias, the net effect of using the accurate fitting formula enhances the redshift power spectrum at large μ and at large k , thus spoiling the agreement of the halo model with the simulation.

Considering carefully all the assumptions in the halo model which may cause the discrepancy with the simulation results, we find only one assumption still needs to be checked, i.e. the redshift-space power spectrum of the halos. The halos were assumed to be linearly biased relative to the *linearly evolved matter distribution*, with the velocity distortion fully described by Kaiser's formula. During the non-linear evolution both assumptions about the redshift-space power spectrum of the halos may break down. Here we check the assumptions with the help of the N-body simulations of the box size $100 h^{-1} \text{ Mpc}$ of Jing & Suto (1998). A comparison of the real space power spectrum of the halos in the simulations with equation (13) for halo masses around $M = 3 \times 10^{11} M_{\odot}$ (the halos around this mass are most important for the two-halo term) are shown in the upper panel of Figure 6, where the fitting formula of Jing (1998) is used for the linear bias factors $b(M)$. Overall, equation (13) gives a reasonable approximation for the real space power spec-

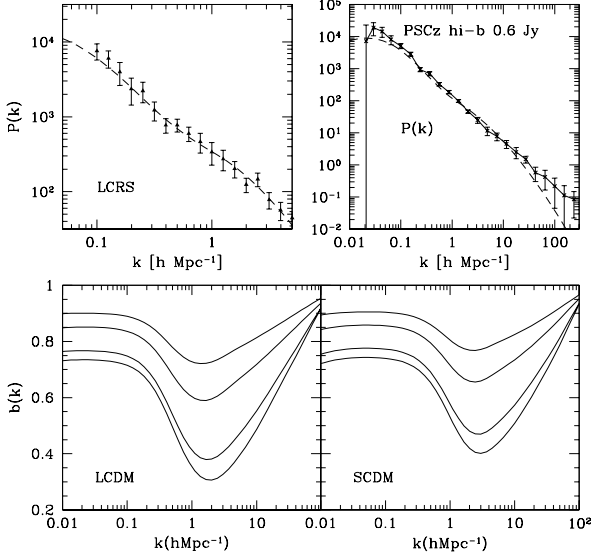


Figure 8. Upper panels — the real-space power spectrum of galaxies. The left panel is for the optical galaxies of the Las Campanas Redshift Survey (the data from Jing & Börner 2001) and the right panel is for the IRAS galaxies of the PSCz survey (the data from Hamilton & Tegmark 2000). The dashed lines are the predictions of the LCM model with $\alpha = 0.08$ in the left panel and 0.25 in the right panel. Lower panels — the scale dependent bias $b(k)$ predicted by the cluster weighted bias model for the two CDM models. From top to bottom, the value of α are $0.08, 0.13, 0.25, 0.32$.

trum of halos in the simulations of both CDM models, with the difference less than a factor of 2. More precisely, for the small scales $k \sim 2h\text{Mpc}^{-1}$ the simulation results are about a factor of 2 higher than the adopted formula in the LCM, but the difference between equation (13) and the simulations is much smaller in the SCDM model. From these comparisons, we are sure that the differences in the real-space power spectrum between the simulations and the adopted simple formula cannot fully account for the discrepancy found for the redshift space power spectrum in Figure 4.

The final possible cause for the discrepancy is that the redshift distortion of halos is not precisely described by Kaiser’s formula. Now we check the power spectrum of halos in redshift space using the simulation data of Jing & Suto (1998). Some typical examples (the symbols) are shown in the lower panels of Figure 6. For comparison, the linear prediction of equation (18) is plotted (the dotted lines), where the real-space power spectrum from the simulations is used for $P^R(k, M_1, M_2)$. The linear prediction is much higher than the simulation results for larger values of μ . Obviously, the redshift distortion of halos is not well described by Kaiser’s formula. The result is not surprising, as we have noted that the peculiar velocity of massive halos deviates typically from the prediction of linear theory by $\sim 30\%$ (Colberg et al. 1998). We parameterize the non-linear peculiar velocity effect by a Lorentz damping factor,

$$P^S(k, \mu, M_1, M_2) = \frac{P_{hh}^R(k, M_1, M_2)}{1 + (k\mu\sigma_h)^2/2} [1 + \Omega^{0.6}\mu^2/b(M_1)]$$

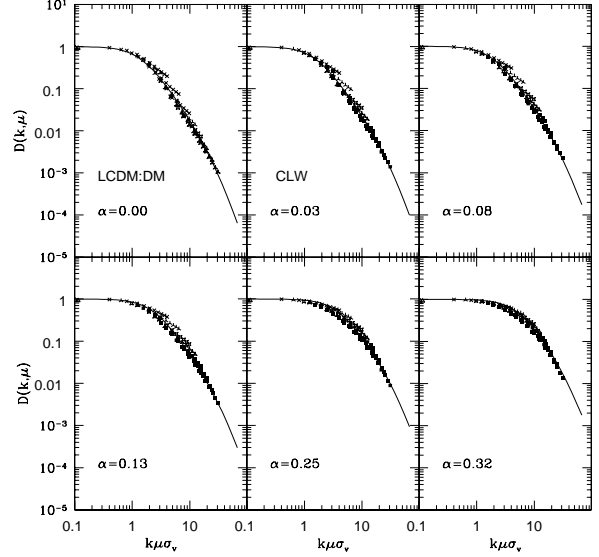


Figure 9. The damping factor $D(k, \mu, \alpha)$ for the LCM model. The solid lines are our fitting formula (Equation 23) with σ_v fixed to 1100 km s^{-1} . The values of α are inserted in each plot

$$\times [1 + \Omega^{0.6}\mu^2/b(M_2)] . \quad (20)$$

where σ_h is a parameter characterizing the pairwise velocity dispersion of halos. The parameter σ_h may be a function of halo mass M_1, M_2 and k , but Sheth & Diaferio (2001) show that σ_h is insensitive to the halo mass. So here we treat it as a constant. This is a valid approximation, as shown in Figure 6. The dashed lines in the lower left panel and the long-dashed lines in the lower right panel agree quite well with the simulation results. The corresponding σ_h values are 200 km s^{-1} for the LCM model and 300 km s^{-1} for the SCDM model, qualitatively consistent with the findings of Colberg et al. (1998). In the upper panel of Figure 7 we present the redshift power spectrum for dark matter using the three modifications discussed above: the modified Press-Schechter function, the modified halo bias (including the non-linear bias from the simulation), and the non-linear peculiar velocity of halos. The result is in very good agreement with the simulation result of $P^S(k, \mu)$ at all scales (with a difference less than a factor of 2).

In a recent paper, Padilla & Baugh (2002) studied the power spectrum of galaxy clusters in redshift space using large N-body simulations. They found that there is no damping of the power spectrum at high wavenumber in redshift space. It is difficult to make direct comparison between our results and theirs because the halos they used in their analysis are only massive ones, which are separated by large distances and the nonlinear effects may be insignificant.

5 THE POWER SPECTRUM OF GALAXIES

This halo model can be readily extended to the real-space and redshift-space power spectra for galaxies if we assume a model for the number of galaxies N per halo of mass M (or the halo occupation number). It was shown by Jing, Mo &

| Model | A_1 | γ_1 | η | A_2 | γ_2 |
|-------|-------|------------|-----------------------|-------|------------|
| SCDM | 4.43 | 0.84 | 5.44×10^{-3} | 8.27 | 0.90 |
| LCDM | 8.41 | 1.05 | 6.75×10^{-4} | 9.22 | 0.84 |

Table 1. The fitting values of the coefficients in Equation 23

Börner (1998) that the LCDM model with a power-law halo occupation number model,

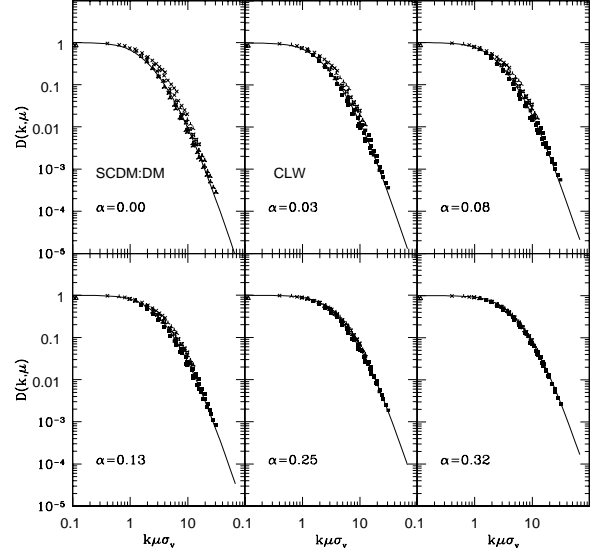
$$N/M \propto (M/M_0)^{-\alpha} \quad (21)$$

can accurately explain the observed two-point correlation function and the pairwise velocity dispersion of the galaxies in the Las Campanas Redshift Survey, where $\alpha = 0$ for $M \leq M_0$, and $\alpha = 0.08$ for $M \geq M_0$ and M_0 is $6 \times 10^{11} h^{-1} M_\odot$. Since α is positive for $M \geq M_0$, i.e. the number of galaxies per unit dark matter mass within a massive halo decreases with the halo mass, JMB98 called this model the cluster-(under)weighted model. They also noted that this parameterization is consistent with the observed trend of Carlberg et al. (1996) for the CNOC clusters. In upper left panel of Figure 8, we compare our result with the real space power spectrum of the Las Campanas Redshift Survey (LCRS). The dashed line is our result for LCDM model and the value of α is 0.08. There is good agreement on all the scales.

It has been recently shown that this model can also successfully describe the clustering of the IRAS galaxies in the PSCz catalog when a higher $\alpha \approx 0.25$ is assumed (Jing, Börner, & Suto 2001; Scoccimarro & Sheth 2001). The upper right panel of Figure 8 shows a comparison of the halo model with the real space power spectrum measured by Hamilton & Tegmark (2000) for the survey. In the figure a value of $\alpha = 0.25$ is assumed, and the model power spectrum is in good agreement with the observed result. Although the spatial bias of the IRAS galaxies is scale-dependent compared with the predictions of CDM models as Hamilton & Tegmark (2000) emphasized, such non-trivial properties of the spatial bias are actually predicted by the cluster weighted halo model (see also Jing et al. 1998). The scale-dependent bias $b(k) = (P(k, \alpha)/P(k, \alpha = 0))^{1/2}$ is plotted in the lower panels of Figure 8 for several choices of α in the two CDM models. The bias factor has a nontrivial dependence on scale for $k > 0.1 h \text{Mpc}^{-1}$. It could be regarded as scale-invariant (or a linear bias) only on larger scales. Since many observation, like the dynamical measurement of β based on measuring the peculiar velocity and spatial distribution of galaxies, rely on the assumption of a linear bias, it is very important to note that such observations must be carried out on sufficiently large scales (also see Seljak 2001).

We also calculate the redshift space power spectrum of galaxies for α varying from 0.03 to 0.32. The analytical result (the lower panels of Figure 7) agrees pretty well with the simulation result of JB2001 for the same cluster-weighted model, where $\alpha = 0.08$ is taken. Following JB2001, we consider the damping factor

$$D(k, \mu, \alpha) = \frac{P^S(k, \mu, \alpha)}{P^R(k, \alpha)(1 + \beta\mu^2)^2}. \quad (22)$$

**Figure 10.** The same as Figure 9, but for SCDM model.

which describes the non-linear motion effect on the redshift power spectrum. We have fitted the scaled damping factor with the following form

$$D(k, \mu, \alpha) = \frac{1}{1 + \frac{1}{2}f(\alpha)(k\mu\sigma_v)^2 + \eta g(\alpha)k\mu\sigma_v^4}. \quad (23)$$

which takes into account the fact that the damping function is approximately a scaling function of $k\mu\sigma_v$. $f(\alpha)$ and $g(\alpha)$ have the forms $e^{-A_1\alpha^{\gamma_1}}$ and $e^{-A_2\alpha^{\gamma_2}}$ respectively. The fitting values for the parameters are given in Table 1 for the two cosmological models. The effective pairwise velocity dispersion is $f^{1/2}(\alpha)\sigma_v$, (where σ_v is the velocity dispersion corresponding to $\alpha = 0$, i.e. $f(0) = 1$), which describes how the velocity dispersion changes with the parameter α . Also note that $f(\alpha)$ depends on the cosmological model and the power spectrum. In our model for dark matter, the effective pairwise velocity dispersion decreases by 40% when σ_8 changes from 1 to 0.7. The formula can also be used to compare the theoretical models with the statistic in large redshift surveys of galaxies.

This CLW model has been shown to be qualitatively consistent with the semi-analytical models of galaxy formation which take into account star formation (Sheth et al. 2001; White 2001). This type of model has been applied to CDM models to predict various statistics for the galaxy clustering (Jing, Mo & Börner 1998; Peacock & Smith 2000; Seljak 2000; Scoccimarro et al. 2000; Berlind & Weinberg 2001). The good agreement shown above means that the halo model can be successfully applied to predict the power spectrum of various galaxies once their halo occupation number model is specified. Thus insight on the galaxy formation can be obtained from measuring the clustering of different populations of galaxies.

6 DISCUSSION AND CONCLUSIONS

In this paper we present an analytical model for the non-linear redshift-space power spectrum of dark matter and of galaxies based on a halo prescription. The model has three important ingredients: the halo mass function, the mass density profile of halos, and the halo-halo redshift space power spectrum. The predicted redshift power spectrum is found to be insensitive to the details of the halo density profiles: the NFW density profile and a steeper inner density profile (Jing & Suto 2000) yield an indistinguishable redshift power spectrum. When we use, as many others have done (for the real space correlation function of dark matter and for the radial averaged redshift power spectrum) the Press-Schechter formula for the halo mass function, the Mo & White formula for the halo bias, and Kaiser's formula for the redshift distortion of the halo spatial distribution, we find that the predicted redshift-space power spectrum for dark matter is too high at large μ to be consistent with the high-resolution simulation results of JB2001. The reason why the halo model works well for the real space clustering but not for the redshift-space power spectrum is that in the latter case the result is dominated by the two-halo term on non-linear scales.

We have checked carefully which assumptions have caused the discrepancy between the halo model prediction and the simulations. First the fitting formulae of the halo mass function and the halo bias from numerical simulations (Sheth & Torman 1999) are used in the replacement of the analytical formulae based on the Press-Schechter formalism. This deteriorates the agreement between the halo model prediction and the simulation results, because there are more small halos and the spatial clustering of small halos is stronger in the modified formulae. We also found that the bias of the halo distribution is nearly linear relative to the linear density field, so the non-linearity of the bias could not be the main contribution to the discrepancy. Instead we found that the non-linear motions of the halos, which were neglected in previous studies, are the main cause. Once we take this effect into account the redshift power spectrum based on the halo model agrees very well with the simulation results. Furthermore, the redshift space power spectrum can be precisely predicted if the halo occupation number model, e.g. the cluster weighted model, is given for the galaxies.

Our results show for the first time that the two-halo term can dominate some statistics in the redshift space even at small scales. Therefore a halo model based on the density profiles of halos and on the redshift distribution of halos predicted by the *linear theory* may become inaccurate for some statistics of redshift clustering. For the time being, an accurate model (analytical or fitting) for the redshift power spectrum of the halos, which includes the effects of the non-linear bias and the non-linear motions, is needed for the prediction of the redshift space power spectra of galaxies and dark matter.

In combination with the cluster weighted bias model, we show that a non-trivial scale-dependent bias is generally expected for galaxies in CDM models. The bias could be regarded linear only on the scales at the wavelength larger than $60h^{-1}\text{Mpc}$ (also see Seljak 2001). The bias is different for different populations of galaxies as observed. The currently favored ΛCDM model can well explain the observed features of the spatial bias reported for optical galaxies and

for IRAS galaxies recently, if the cluster weighted bias model is applied.

7 ACKNOWLEDGMENTS

The work is supported in part by the One-Hundred-Talent Program, by NKBRF(G19990754), by NSFC(No.10043004), and by SFB375. We thank an anonymous referee for helpful comments.

REFERENCES

- Ballinger, W. E., Peacock, J. A., & Heavens, A. F. 1996, MNRAS, 282, 877
- Bean, A. J., Ellis, R. S., Shanks, T., Efstathiou, G., & Peterson, B. A. 1983, MNRAS, 205, 605
- Berlind, A. A., & Weinberg, D. H. 2001, astro-ph/0109001
- Bond, J. R., Cole, S., Efstathiou, G., & Kaiser, N. 1991, ApJ, 379, 440
- Bower, R. G. 1991 MNRAS 248, 332
- Bromley, B. C., Warren, M. S. & Zurek, W. H. 1997, ApJ, 475, 414
- Carlberg, R. G., Yee, H. k. C., Ellingson, E., Abraham, R., Gravel, P., Morris, S., & Pritchet, C. J. 1996, ApJ, 462, 32
- Colberg et al. 2000, MNRAS, 313, 229
- Cole, S., Fisher, K. B., Weinberg, D. H. 1994, MNRAS, 267, 785
- Cole, S., Fisher, K. B., Weinberg, D. H. 1995, MNRAS, 275, 515
- Cole S., Lacey C. G. 1996, MNRAS, 281, 716
- Cooray, A. astro-ph/0105440
- Cooray, A., Hu, W., & Miralda-Escude, J. 2000, ApJ, 535, L9
- Davis, M., Peebles, P. J. E. 1983, ApJ, 267, 465
- Diaferio, A. & Geller, M. J. 1996, APJ, 467, 19
- Fisher K. B., Davis M., Strauss M. A., Yahil A., & Huchra J. P. 1993, ApJ, 402, 42
- Fukushige, T., & Makino, J. 1997, ApJ, 477, L9
- Fukushige, T., & Makino, J. 2001, ApJ, 557, 533
- Geller, M. J., Peebles, P.J.E. 1973, ApJ, 184, 329
- Hamana, T., Yoshida, N., Suto, Y., & Evrard, A. E. 2001, ApJ, 561L, 143
- Hamilton, A. J. S., & Tegmark, M. 2002, MNRAS, 330, 506
- Jenkins, A., Frenk, C. S., White, S. D. M., Colberg, J. M., Cole, S., Evrard, A. E., Couchman, H. M. P. & Yoshida, N. 2001, MNRAS, 321, 272
- Jing, Y. P. 1998, ApJ, 503L, 9
- Jing, Y. P. 1999, ApJ, 515L, 45
- Jing, Y. P., Börner G. 2001, MNRAS, 325, 1389
- Jing, Y. P., Börner G., Suto, Y. 2002, ApJ, 564, 15
- Jing, Y. P., Mo, H. J., & Börner G. 1998, ApJ, 494, 1
- Jing, Y. P., & Suto, Y. 2000, ApJ, 529, L69
- Kofman L., Gnedin N., Bahcall N. 1993, ApJ, 413, 1
- Kaiser, N. 1987, MNRAS, 227, 1
- Klypin, A., Kravtsov, A. V., Bullak, J. S., & Primack, J. R. 2001, ApJ, 554, 903
- Lee, J., & Shandarin, S. F. 1998, ApJ, 500, 14
- Lokas, E. L. 2001, MNRAS, 327, 21
- Ma, C. & Fry, J. N. 2000a ApJ, 531L, 87
- Ma, C. & Fry, J. N. 2000b ApJ, 543, 503
- Magira, H., Jing, Y. P. & Suto, Y. 2000, ApJ, 528, 30
- Matsubara, T., & Suto, Y. 1996, ApJ, 470L, 1
- McClelland, J., & Silk, J. 1977, ApJ, 217, 331
- Mo, H. J., Jing, Y. P., & Börner G. 1997, MNRAS, 286, 979
- Mo, H. J., Jing, Y. P., & White, S. D. M. 1997, MNRAS, 284, 189
- Mo, H. J., & White, S. D. M. 1996, MNRAS, 282, 347
- Moore, B., Governato, F., Quinn, T., Stadel, J., & Lake, G. 1998, ApJ, 499, L5
- Moore, B., Quinn, T., Governato, F., Stadel, J., & Lake, G. 1999, MNRAS, 310, 1147
- Navarro, J.F., Frenk, C.S., & White, S.D.M. 1996, ApJ, 462, 563
- Navarro, J.F., Frenk, C.S., & White, S.D.M. 1997, ApJ, 490, 493
- Neyman, J., & Scott, E. L. 1952, APJ, 116, 144
- Padilla, N. D., & Baugh, C. M. 2002, MNRAS, 329, 431
- Peacock, J.A., Dodds, S.J. 1994, MNRAS, 267, 1020
- Peacock, J.A., Dodds, S.J. 1996, MNRAS, 280, L19
- Peacock J. A., 1992, In Martinez V., Portilla M., Sáez D., eds, New insights into the Universe, Proc. Valencia summer school (Springer, Berlin), P1
- Peacock, J. A., & Smith, R. E. 2000, MNRAS, 318, 1144

- Peacock, J. A. et al. 2001, *Nature*, 410, 169
- Peebles, P. J. E. 1974, *A&A*, 32, 197
- Peebles, P. J. E. 1980, *The Large Scale Structure of the Universe* (Princeton University Press: Princeton)
- Press, W. H., & Schechter, P. 1974, *ApJ*, 196, 1
- Scherrer, R. J. & Bertschinger, E. 1991, *ApJ*, 381, 349
- Scoccimarro, R., Sheth, R. K., Hui, L., & Jain, B. 2001, *ApJ*, 546, 20
- Scoccimarro, R., & Sheth, R. K. 2002, *MNRAS*, 329, 629
- Seljak, U. 2000, *MNRAS*, 318, 203
- Seljak, U. 2001, *MNRAS*, 325, 1359
- Seto, N. & Yokoyama, J. i. 1998, *ApJ*, 492, 421
- Sheth, R. K. 1996, *MNRAS*, 279, 1310
- Sheth, R. K., Hui, L., Diaferio, A. & Scoccimarro, R. 2001, *MNRAS*, 325, 1288
- Sheth, R. K. & Jain, B. 1997, *MNRAS*, 285, 231
- Sheth, R. K., Mo, H. J., & Tormen, G. 2001, *MNRAS*, 323, 1
- Sheth R. K. & Tormen G. 1999, *MNRAS*, 308, 119
- Suto, Y., Magira, H., Jing, Y. P., Matsubara, T., & Yamamoto, K. 1999, *PThPS*, 133, 183
- White, M. 2001, *MNRAS*, 321, 1